CRYSTAL GROWTH & DESIGN

Article

Cite This: Cryst. Growth Des. 2019, 19, 932−941

pubs.acs.org/crystal

Kinetic Study for Comprehensive Understanding of Solid-State Polymorphic Transitions of Nicotinamide/Pimelic Acid Cocrystals

Yong Joon Lee,[†] Olga Pahom,[‡] and Brandon L. Weeks*[,†]

[†]Department of Chemical Engineering and [‡]Department of Classical and Modern Languages and Literatures, Texas Tech University, Lubbock, Texas 79409, United States

Supporting Information

ABSTRACT: Solid-state polymorphic transition (SSPT) has been regarded as an interesting research subject for a long time, but kinetics and the mechanism of these phase transitions are still not fully understood. Particularly, kinetic studies on the SSPT process of cocrystals are not widely reported even though extensive novel cocrystal polymorphs have been discovered over the recent decades. Herein we presented a comprehensive kinetic study of the enantiotropic polymorphic system of 1:1 nicotinamide (NA)−pimelic acid (PA) cocrystals with the combination of various analytical methods. Bulk kinetic studies conducted with powder X-ray diffraction and differential scanning calorimetry indicated that both directions of SSPT (form 1 ↔ form 2) occur by a nucleation and growth mechanism. In addition, large activation energy barriers of form 1 → form 2 with a wide range (337.1−514.2 kJ mol^{-1}) and variations in the onset transition temperature were observed, depending on the crystal conditions. In situ atomic force microscopy analysis was also carried out to monitor the surface morphology change at the nanoscale to supplement the bulk kinetics.

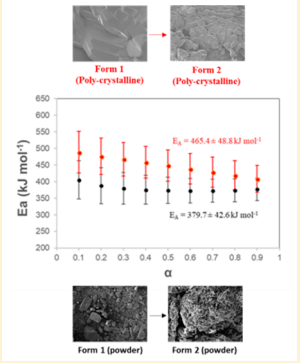

1. INTRODUCTION

Crystal engineering and supramolecular chemistry involve the design of appropriate molecular solid forms to obtain desired properties.[1−5] In the pharmaceutical industry, various crystal solid-state forms such as polymorphs, salts, cocrystals, hydrates, and solvates have been studied for the enhancement of biocompatibility, solubility, dissolution rate, and mechanical properties of active pharmaceutical ingredients.[1,3,5−10] A key characteristic of crystalline materials that is relevant to these research areas is polymorphism. Polymorphism is defined as phenomena observed in compounds that have more than one crystal structure arising from a different arrangement of molecules in the crystal structure.[1] It is estimated that more than half of pharmaceuticals have at least two polymorphic forms which may have different biological effects.[11,12]

Polymorphic systems are governed by both thermodynamics and kinetics. The system ultimately moves to the most thermodynamically stable state under given conditions (temperature and pressure), while the rate and the pathway to the final state of the polymorph are determined by kinetics. In order to selectively produce polymorphic forms of materials with desired properties and to avoid product failure caused by unexpected solid-state polymorphic transitions (SSPT), researchers have sought to develop effective polymorph screening methods and to investigate the thermodynamic stability of these polymorphs.[13−20] In terms of the kinetics, only limited studies have been reported.[21−31] This might be due to the long time scales required for SSPT experiments, derived from relatively high energy barriers. The factors that determine the kinetics are still not fully understood, and there is ongoing debate centered on two proposed kinetic mechanisms,[32−34] "nucleation and growth theory"[21,22,35] and "displacive or cooperative motion".[36,37]

It was once misunderstood that cocrystallization can be used to prevent the undesired polymorphic form.[38] In recent years, however, numerous cocrystal polymorphs have been reported as the demands to enhance drug performance and protect intellectual property have increased.[38−44] According to surveys conducted by Aitipamula and co-workers, the percentage of cocrystals which have polymorphs is almost the same as that of single component crystals.[38] Most studies have focused on identifying their new polymorphs and revealing their crystal structure changes upon polymorphic transition. However, a comprehensive understanding of kinetics of polymorphic transition is essential not only for fundamental reasons but also for the successful application of novel pharmaceutical cocrystals.

In this work, 1:1 nicotinamide (NA)/pimelic acid (PA) cocrystal was used as a model system to reveal the SSPT mechanism and to determine whether traditional kinetic models can be applied to cocrystals during solid−solid phase transitions. NA and PA are widely used as cocrystal formers for cocrystallization of active pharmaceutical ingredients.[44] It has been reported that the 1:1 NA/PA cocrystal has two enantiotropically related polymorphic forms.[44] Form 1, triclinic, is thermodynamically stable at room temperature.[44] Form 2, orthorhombic, is stable above ∼94 °C.[44] In crystallography, polymorphs of NA/PA cocrystal can be

Received: October 2, 2018
Revised: December 21, 2018
Published: January 9, 2019

DOI: 10.1021/acs.cgd.8b01488
Cryst. Growth Des. 2019, 19, 932−941

classified as conformational polymorphs where the crystal structure of the two forms is different with respect to molecular conformation of both NA and PA molecules in the crystal lattice. One of the reasons we used NA/PA cocrystal as a model system is precisely because most known cocrystal polymorphs are categorized as conformational polymorphs.[38] Another reason for choosing the NA/PA cocrystal in this study is that the time scale of the SSPT process of a NA/PA cocrystal is appropriate for experimental kinetic studies.

The combination of three analytical techniques were used in this work: powder X-ray diffraction (PXRD), differential scanning calorimetry (DSC), and atomic force microscopy (AFM). PXRD and DSC have been used as conventional tools for bulk kinetics of phase transitions. PXRD was used for investigating the SSPT mechanism of NA−PA cocrystals by fitting the experimental data to several kinetic models which have been previously appreciated in the solid-state reaction kinetics study.[45] Thermal analysis using DSC was used to obtain kinetic parameters and insight into the dependence of the crystal sizes and crystal forms (powders and polycrystalline) on the kinetics and energy barrier of transitions.

In phase transition studies, AFM is very useful because it can trace the morphology change in real time at the nanometer scale without additional sample preparation which can induce unwanted changes. There have been several reports that used AFM to attain some kinetic parameters and to study the phase transition mechanism.[46−53] These studies were mostly related to solid-state surface reactions which are governed by the interaction of the solid surface with its environment, such as the hydration, solvation, dehydration, and desolvation process. We employed an in situ AFM technique to supplement the bulk kinetic analysis with PXRD and DSC and to observe the surface morphology change during the solid-state polymorphic transitions.

2. EXPERIMENTAL SECTION

2.1. Materials. A 1:1 stoichiometric ratio of form 1 of NA/PA cocrystal was prepared by dissolving 200 mg (1.64 mmol) of NA (Alfa Aesar) and 262.4 mg (1.64 mmol) of PA (Alfa Aesar) in a 1 mL of methanol without further purification.[44] A 1:1 stoichiometric ratio of form 2 of NA/PA cocrystal was prepared by dissolving a 200 mg (1.64 mmol) of NA and 131.2 mg (0.82 mmol) of PA in a 1 mL of methanol.[44] The mixture was vigorously vortexed for 15 min with an S8220 deluxe tube mixer (American Scientific Products). Subsequently, the solvent in the solution was evaporated slowly at room temperature. After 1−2 days, plate-like polycrystalline samples of form 1 and form 2 were generated.

PXRD and DSC experiments were performed to confirm the identities of two forms of cocrystals. Crystals grown from the mother liquor were dried on a filter paper at room temperature for 2 h before characterization. PXRD experiments were conducted on a Rigaku Ultima III diffractometer with Cu−Kα radiation operating in parallel-beam geometry, voltage 40 kV, and current 44 mA, and scanned within the range of $2\theta = 3-50°$ at a scan rate of 1.5 deg min^{-1}. Before scanning, polycrystalline samples were manually ground to make crystalline powder form, and the size of the crystals was measured using scanning electron microscopy (SEM) analysis ($\lesssim$100 μm). The patterns of each form at room temperature were well matched to the simulated patterns registered in the Cambridge Structural Database (CSD) and those reported in the literature[44] (see Supporting Information, Figure S1). Note that the appearance of a few peaks observed in PXRD, not corresponding to simulated patterns, is related to the individual components of the cocrystal (e.g., form 1 at 2θ = 45°). The peaks related to impurities were excluded for the kinetic studies.

In DSC experiments, a TA Instruments model Q20 was used. A total of 3−5 mg of each polycrystalline samples was heated in a crimped aluminum pan in the range of 2−115 °C at a constant heating rate of 1 K min^{-1} under a nitrogen environment (50 mL min^{-1}). Before running, indium standards were used for calibration purposes. For the data analysis, TA universal analysis 2000 software was used. The DSC curves of the two forms correspond to those reported in the previous literature[44] (see Supporting Information, Figure S2). In the DSC curve for form 1, a small endotherm peak for form 1 → form 2 transition was observed at 94.6 ± 0.2 °C, followed by the appearance of an endotherm peak of fusion at 109.8 ± 0.1 °C. The calculated enthalpy change of polymorphic transition was 9.1 ± 0.3 kJ mol^{-1}. In the DSC curve for form 2, only an endotherm peak of fusion appeared at 109.8 ± 0.1 °C.

2.2. Powder X-ray Diffraction (PXRD). Kinetic transition experiments for form 1 → form 2 at 94 ± 1 °C were investigated with PXRD analysis. Form 1 powders ($\lesssim$100 μm) were mounted on a sample holder and kept in a conversional oven at a temperature of 94 ± 1 °C. Samples were taken out from the oven every 30 min and scanned by PXRD. Because the transition rate of the reverse transition (form 2 → form 1) is very slow, the impact of the reverse transition during scanning was assumed to be negligible. PXRD experiments for SSPT of form 2 → form 1 at room temperature (20 °C) and 40 °C were also conducted in the same conditions at prearranged time intervals. Powders of form 2 ($\lesssim$100 μm) were prepared by heating form 1 in the oven at 96 °C for 16 h. Each run was repeated two times.

PXRD measurements were analyzed with MDI Jade 9 software to proceed isothermal kinetic modeling study. Relative peak intensity changes at three points ($11.0 \le 2\theta \le 11.4$, $12.1 \le 2\theta \le 12.5$, $19.4 \le 2\theta \le 20.0$) were collected to obtain the fractional conversion (α) at each measured time. The two peaks at $11.0 \le 2\theta \le 11.4$ and $19.4 \le 2\theta \le 20.0$ represent the existence of form 2, while the peak at $12.1 \le 2\theta \le 12.5$ depicts the existence of form 1. Thus, the fractional conversion of form 1 at the measured time ($\alpha_{\text{form1}\rightarrow\text{form2},\,t}$) during form 1 → form 2 at 94 °C was calculated by

$$\alpha_{\text{form1}\rightarrow\text{form2},t} = \frac{\frac{I_{11.2,t}}{I_{11.2,tf}} + \frac{I_{19.7,t}}{I_{19.7,tf}} + \frac{(I_{12.3,t_i} - I_{12.3,t})}{I_{12.3,t_i}}}{3} \quad (1)$$

where $I_{11.2,t}$, $I_{12.3,t}$, and $I_{19.7,t}$ are integrated PXRD peak areas at approximately $11.0 \le 2\theta \le 11.4$, $12.1 \le 2\theta \le 12.5$, and $19.4 \le 2\theta \le 20.0$ at measured time (t) respectively, $I_{11.2,ti}$, $I_{12.3,ti}$, and $I_{19.7,ti}$ are integrated PXRD peak areas at initial time (t_i), and $I_{11.2,tf}$, $I_{12.3,tf}$, and $I_{19.7,tf}$ are integrated PXRD peak areas when the old phase is completely converted into a new phase (t_f).

In the same manner, the fractional conversions of form 2 at the measured time ($\alpha_{\text{form2}\rightarrow\text{form1},\,t}$) during the reverse transition at 20 and 40 °C were calculated as

$$\alpha_{\text{form2}\rightarrow\text{form1},t} = \frac{\frac{I_{12.4,t}}{I_{12.4,tf}} + \frac{(I_{11.2,t_i} - I_{11.2,t})}{I_{11.2,t_i}} + \frac{(I_{19.7,t_i} - I_{19.7,t})}{I_{19.7,t_i}}}{3} \quad (2)$$

2.3. Differential Scanning Calorimetry (DSC). Thermal analysis with DSC was conducted with a Q20 RSC90 (TA Instruments) for the calculation of activation energy of form 1 → form 2 transition using powder ($\lesssim$100 μm) and polycrystalline samples (100−500 μm); for the comparison between powders and poly crystalline of kinetics of form 2→ form 1 transition at isothermal conditions (20 °C); and for the observation of DSC pattern changes for form 1 → form 2 transition of initial polycrystalline upon several heating/cooling cycles. Non-isothermal kinetic runs at different constant heating rates (0.1, 0.5, 1, 2, and 3 K min^{-1}) on both powder and polycrystalline of form 1 were carried out for kinetic analysis of form 1 → form 2 transitions. Each run was repeated 3−5 times, and 2−4 mg of powder and polycrystalline were used. Before each run, indium standards were used for calibration purposes. In the experiments, samples grown from the same batch were used to minimize sample variations (crystal size and impurities). Kinetic data

DOI: 10.1021/acs.cgd.8b01488
Cryst. Growth Des. 2019, 19, 932−941

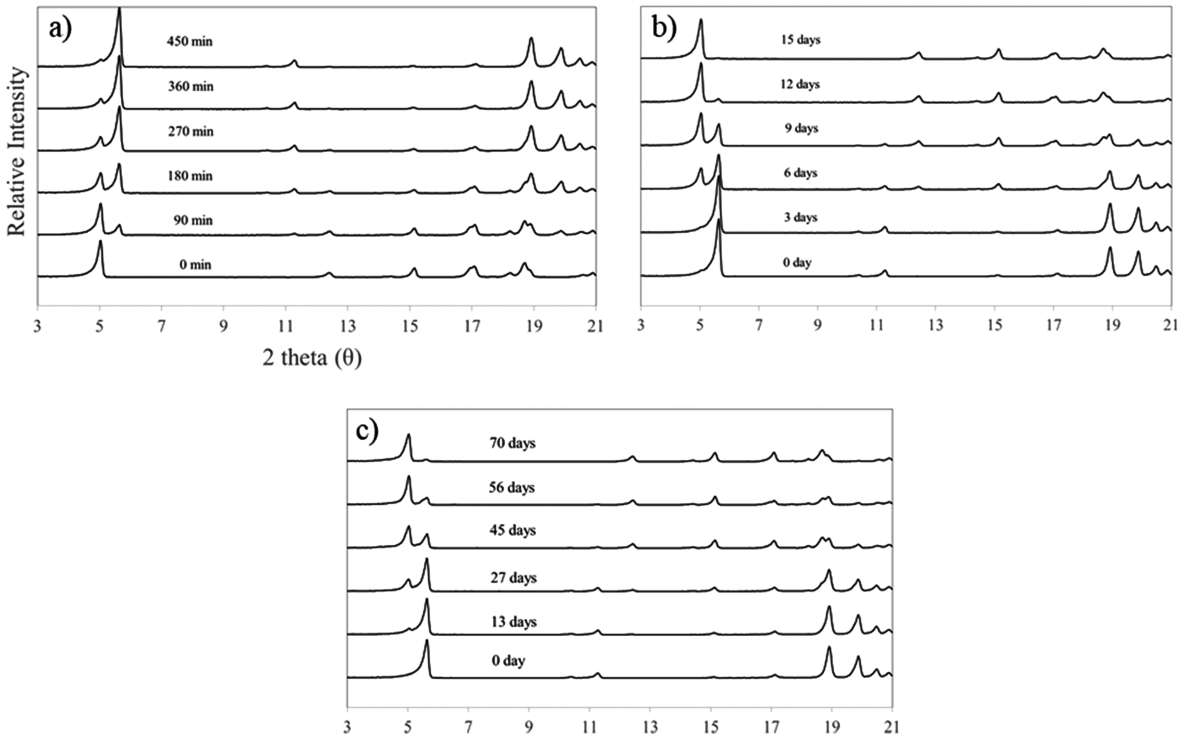

Figure 1. Change of PXRD patterns with time during polymorphic transition of (a) forward transition (form 1 → form 2) at 94 °C; (b) reverse transition (form 2 → form 1) at 20 °C; (c) reverse transition (form 2 → form 1) at 40 °C.

collection and analysis were performed, based on the ICTAC kinetics committee recommendations.[54,55]

2.4. Scanning Electron Microscopy (SEM). The surface morphology of polycrystalline and powder of NA/PA cocrystals was observed with a Hitachi 3400 scanning electron microscope, and the size of the crystals of two types of samples was measured (Supporting Information, Figure S3). To obtain high resolution images, all samples were precoated by a thin layer of gold (~5 nm) before imaging.

2.5. Atomic Force Microscopy (AFM). Atomic force microscopy (Bruker Multimode 8 with a heating stage) measurements were conducted in situ by increasing the temperature gradually from room temperature to 94 °C for observation of surface morphology change during form 1 → form 2 transition. Polycrystalline form 1 was fixed on an AFM sample stage with double-sided adhesive tape. Subsequently, each image was scanned in contact mode at the scan rate of 2 Hz as the temperature of the sample stage was controlled. Scan size was 10 μm × 10 μm. Collected images were analyzed with Nanoscope Analysis 1.7.

3. RESULTS AND DISCUSSION

3.1. Kinetic Transition Experiment with PXRD. Figure 1a shows the change of PXRD patterns from form 1 to form 2 with the time when the temperature is held isothermally at 94 °C. The transition temperature of 94 °C was selected based on the DSC experiment (at heating rate: 1 K min^{-1}), where the endothermal peak for the forward transition (form 1 → form 2) was observed. The change of PXRD patterns during the reverse transition (form 2 → form 1) at 20 and 40 °C is also shown in Figure 1b,c. In both experiments, in the forward and reverse transitions, no phase separation of individual component was observed. In the forward transition at 94 °C, it took 8−10 h for form 1 to be completely converted into form 2, and the transition rate increased sharply with rising temperature. On the other hand, the reverse transition was not observable at experimental time scales when the temperature was close to 94 °C. The transition from form 2 → form 1 was experimentally observed when the temperature decreased to 40 °C. However, it was still very slow; it took 70−80 days for form 2 to be completely converted to form 1. The transition rate from form 2 → form 1 gradually tended to increase when the temperature decreased toward room temperature.

In nucleation and growth theory, the phase transition involves two kinetic steps, nucleation and phase propagation. Overall, the transition rate is limited by the nucleation process, and the nucleation rate strongly depends on the nucleation kinetic barrier. The Gibbs free energy change for kinetic nucleation barrier (ΔG_N^*) is expressed as

$$\Delta G_N^* = \frac{16\pi\gamma^3 T_t^2}{3\Delta h^2 (T_t - T)^2} \tag{3}$$

where γ is the surface free energy per unit area, Δh is the enthalpy change of the phase transition, T_t is the thermodynamic transition temperature, and T is the temperature.[56−62] The formation of stable nuclei involves the transfer of one atom or molecule across the interface onto the embryo once the critical-sized embryo is formed. Therefore, the rate of postcritical nuclei formation (N) can be described as

$$N = N_0 \exp\left(-\frac{\Delta G_N^* + G^*}{RT}\right) \tag{4}$$

where N_0 is the preexponential factor and G^* is the activation energy of phase propagation.[57,60−62] The kinetics of phase transition is influenced by phase propagation steps once the stable nuclei are formed, and the rate of phase propagation (n) can be expressed as

$$n = n_0 \exp\left(-\frac{G^*}{RT}\right)\left[1 - \exp\left(-\frac{\Delta G}{RT}\right)\right] \tag{5}$$

DOI: 10.1021/acs.cgd.8b01488
Cryst. Growth Des. 2019, 19, 932−941

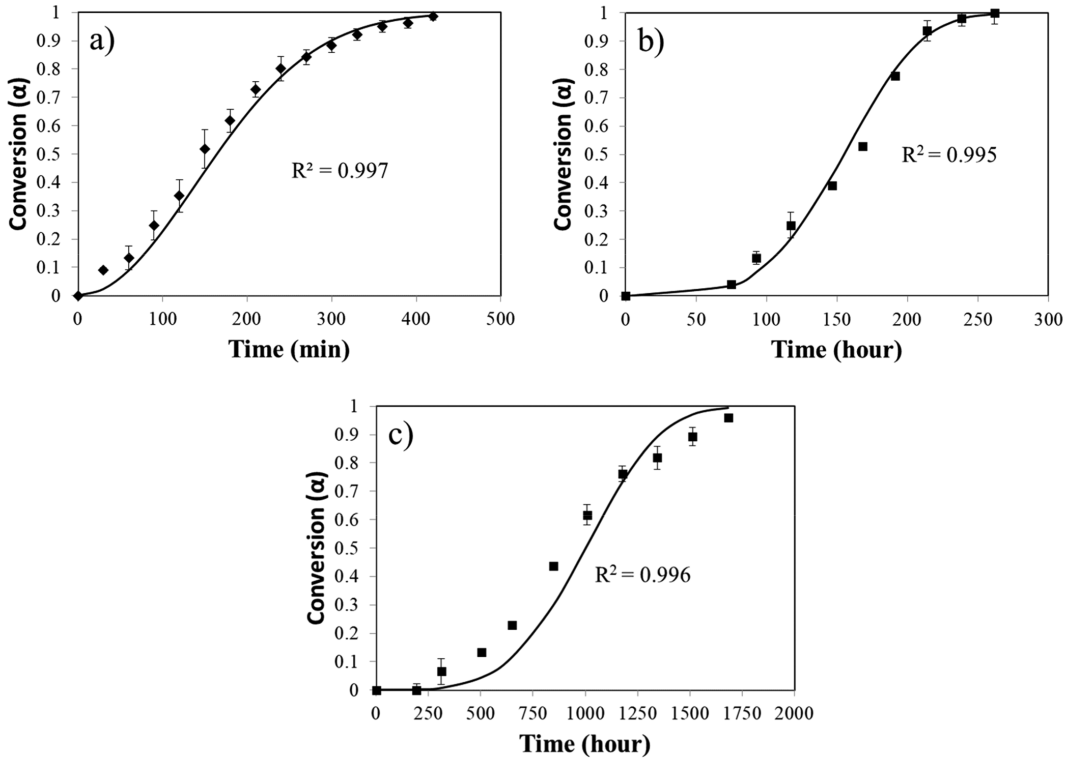

Figure 2. Fractional conversion versus time during polymorphic transition of (a) form 1 → form 2 at 94 °C; (b) form 2 → form 1 at 20 °C; (c) form 2 → form 1 at 40 °C. The solid line represents the best fit model at each transition.

Table 1. Best Fit Kinetic Models and the Temperature-Dependent Rate Constants (k)

	best fit kinetic model	integral form of rate equation	rate constant (min^{-1})
Form 1 → Form 2 @ 94 °C	Avrami–Erofeev (n = 2)	$[-\ln(1-\alpha)]^{1/2} = kt$	$(5.07 \pm 0.11) \times 10^{-3}$
Form 2 → Form 1 @ 20 °C	Avrami–Erofeev (n = 4)	$[-\ln(1-\alpha)]^{1/4} = kt$	$(6.41 \pm 0.11) \times 10^{-5}$
Form 2 → Form 1 @ 40 °C	Avrami–Erofeev (n = 2)	$[-\ln(1-\alpha)]^{1/2} = kt$	$(1.60 \pm 0.05) \times 10^{-5}$

where n_0 is the preexponential factor and ΔG is the difference of the free energy between two phases.[60−62]

Equation 3 indicates that the nucleation process may not occur at the thermodynamic transition point (T_t) where ΔG_N^* becomes infinity. Superheating or supercooling must be involved in a nucleation event to overcome the nucleation energy barrier, and the nucleation barrier decreases with superheating or supercooling. This implies that an actual thermodynamic transition point exists between 40 and 94 °C. However, due to the presence of a large thermal hysteresis between form 1 ↔ form 2 transitions, the determination of T_t was not straightforward in the PXRD experiment. The existence of a large thermal hysteresis was confirmed by the DSC result of three heating/cooling cycles at a constant heating/cooling rate of 0.1 K min^{-1} where the endothermic peak for form 1 → form 2 was only observed at the first heating cycle, whereas no peaks were found at other cycles (see Supporting Information, Figure S4). In general, the existence of a large thermal hysteresis indicates that the phase transition is first order where kinetics are controlled by a nucleation and growth mechanism. It is also noted that a large thermal hysteresis, originated by the variance of nucleation barriers in two opposite directions, is induced by the change of crystal quality such as mosaicity, defects, and surface damage during the transition.

From eq 4 and 5, different temperature-dependent transition rates observed in the forward and reverse transitions could be understood. In the forward transition region ($T > T_t$), where the transition is induced by superheating, the transition rate would rapidly increase when the temperature increases from T_t due to the decrease in ΔG_N^* in eq 4 and the increase in ΔG in eq 5. On the other hand, in the reverse transition region ($T < T_t$), where the transition is induced by supercooling, these effects would be compensated by a decrease in temperature.

For bulk kinetic modeling, conversion-versus-time data were obtained using eqs 1 and 2. As seen in Figure 2, the sigmoidal shape of conversion-versus-time curves was commonly observed in both directions of the transitions. In solid-state reactions, a sigmodal shape is only shown in two isothermal kinetics models, Avrami-Erofeev and Prout-Tompkins, which are nucleation and growth mechanisms.[45] Thus, each set of conversion-versus-time curve was fit to these two kinetic models by least-squares regression of integral forms of rate equations. The best fit model was determined by evaluating three statistical parameters: the standard deviation of the slope of the linear regression curve (S_K), the coefficient of determination of linear regression curve ($R_K{}^2$), and the coefficient of determination (R^2) (see Supporting Information, Table S1). Table 1 shows the best fit kinetic models and calculated temperature-dependent rate constants (k) at each condition of transition. The Avrami models was a good fit to the data in both directions of transitions, but different Avrami parameters (n) were obtained: n = 2 in the forward transition at 94 °C and reverse transition at 40 °C, and n = 4 in the

DOI: 10.1021/acs.cgd.8b01488
Cryst. Growth Des. 2019, 19, 932−941

reverse transitions at 20 °C. It is generally understood that the Avrami parameter is related to the growth dimension and nucleation rates.[45,63] However, the physical interpretation is elusive because the contribution of nucleation and growth to the SSPT process cannot be analyzed separately in bulk kinetics. Therefore, it can be assumed that the deviation in the shape of nucleus and the nucleation rates, owing to different reaction temperatures, might contribute to the difference in the observed values.

3.2. DSC. In the kinetics of solid-state reactions, the rate of reaction is typically expressed as a function of two variables, conversion (α) and temperature.[45,54] When the reaction rate at a constant extent of conversion is assumed to be only dependent on temperature (isoconversional condition), a global activation energy barrier (E_a) of reaction can be obtained by various methods, including Arrhenius relations.[45,54] In the case of kinetics in the SSPT process, isothermal analysis is often inappropriate for determining the activation energy due to limited measurable temperature ranges. Thus, non-isothermal kinetics was carried out with DSC to achieve the overall activation energy of form 1 → form 2 phase transition. Note that the activation energy for the reverse transition, where the phase transition is induced by supercooling, is not measurable with standard Arrhenius kinetics since the reaction rate is not solely dependent on the temperature, as previously described in section 3.1.

Figure 3 shows the DSC curves for form 1 → form 2 transition of polycrystalline and powders of NA/PA cocrystals

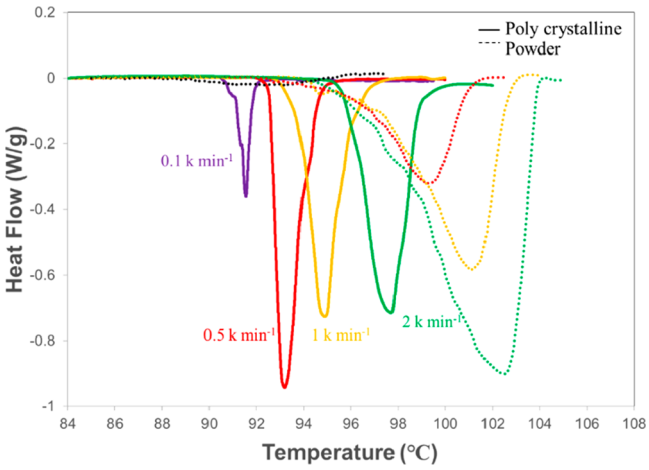

Figure 3. Comparison of DSC curves for polycrystalline and powder form of samples during form 1 → form 2 transition at a different constant heating rate (0.1, 0.5, 1, 2 K min^{-1}).

at a different constant heating rate (0.1, 0.5, 1, 2 K min^{-1}). In both types of samples, the onset and the maximum peak temperature tended to increase as the heating rate increased. The onset temperatures of two types of samples at the same heating rates were quite similar. However, peak widths for the transition of powder samples were much broader than those of polycrystalline samples, which means that further heating should be involved for complete conversion. This might be explained by nucleation and growth theory where nucleation of the new phase starts slowly at the onset temperature, followed by propagation at relatively higher rates. The transition process of powders inevitably involves more nucleation events than that of polycrystalline samples. This could result in larger peak widths and the appearance of several spikes that originated from the different nucleation points of separate crystalline powders. In the case of polycrystalline samples, once the nucleus is formed, the transition rate might be accelerated by faster phase propagation, which leads to relatively smooth and sharp DSC patterns.

Experimental data obtained from each non-isothermal DSC runs at different heating rates were used to obtain fractional conversion-versus-time curves. Then, the global activation energy barrier for form 1 → form 2 transition of polycrystalline and powders was calculated based on the Starink's isoconversional method and the Kissinger approach. In Starink's equation, the kinetics of SSPT is expressed as

$$\ln \frac{\beta}{T_\alpha^{1.92}} = -1.0008 \frac{E_{A,\alpha}}{RT_\alpha} + \text{const} \quad (6)$$

where β is the constant heating rate and T_α is the temperature at specific fractional conversion (α).[54] Figure 4a shows the activation energy barriers (E_a) of polycrystalline and powder samples at specific fractional conversion ($0.1 \leq \alpha \leq 0.9$) obtained by linear least-squares fit of eq 5. The mean values of activation energies of both samples were calculated to be 465.4 ± 48.8 kJ mol^{-1} and 379.7 ± 42.6 kJ mol^{-1} respectively. The decreasing trend of E_a with α was commonly observed in both type of samples. This result is reasonable because the kinetic energy barrier is expected to be reduced as the temperature increases with increasing conversion (eqs 3−5). The same trend was found in the previous result for the polymorphic transition of 4′ hydroxyacetophenone[31] and for the melting of glucose and fructose.[62]

Kissinger's approach is a well-known, simple, kinetic technique to determine the activation energy of solid-state conversion and is described as

$$\ln \frac{\beta}{T_{m,i}^2} = -\frac{E_A}{RT_{m,i}} + \text{const} \quad (7)$$

where $T_{m,i}$ is the temperature where maximum peak appeared in the DSC curve at the ith constant heating rate. The main assumption of the method is that the rate equation for the kinetic model is independent of the heating rates (β).[54] It is known that the kinetic process controlled by Avrami−Erofeev model meets the assumption of the Kissinger equation.[54] From the linear least-squares fit of eq 7, the mean value of activation energies for polycrystalline and powder were calculated to be 458.8 ± 45.2 kJ mol^{-1} and 350.1 ± 23.8 kJ mol^{-1} respectively, which were in agreement with those obtained by Starink's method (Figure 4b).

On the basis of non-isothermal DSC thermal analysis, the result may be summarized as follows. First, a relatively large global activation energy (E_a) of form 1 → form 2 transition in the range of 337.1−514.2 kJ mol^{-1} was observed depending on the sample types (powder and poly crystalline) and the extent of conversion (α). Calculated values were 3−5 times higher than the enthalpy measured during heating of form 1 ($\Delta_{sub}H_m$ = 104.0 ± 15.1 kJ mol^{-1}) obtained by TGA analysis (see Supporting Information, Figure S5). The large variation between these values was previously reported in other kinetic studies,[24,31,64−69] but the relation between E_a and the enthalpy measured with the TGA remains unclear. Mnyukh suggested that molecular rearrangement (phase propagation) occurs at the solid−solid interface in the existence of effective gap by "stimulated sublimation" after nucleation of a new phase is

DOI: 10.1021/acs.cgd.8b01488
Cryst. Growth Des. 2019, 19, 932−941

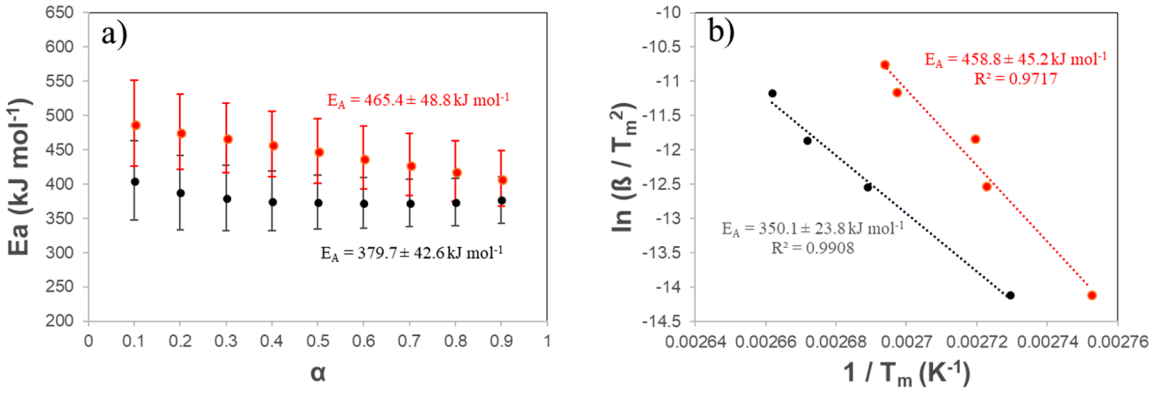

Figure 4. (a) The activation energy barrier (E_a) at specific fractional conversions ($0.1 \leq \alpha \leq 0.9$) for form 1 → form 2 transition of polycrystalline (red) and powder (black) of NA/PA cocrystals, obtained by linear least-squares fits of Starink's eq (eq 6); (b) plots of $\ln(\beta/T_m^2)$ versus reciprocal of the maximum DSC peak temperature ($1/T_m$) for polycrystalline (red) and powder (black) of NA/PA cocrystals. Activation energy barriers of both forms were attained by linear least-squares fits of the Kissinger equation (eq 7).

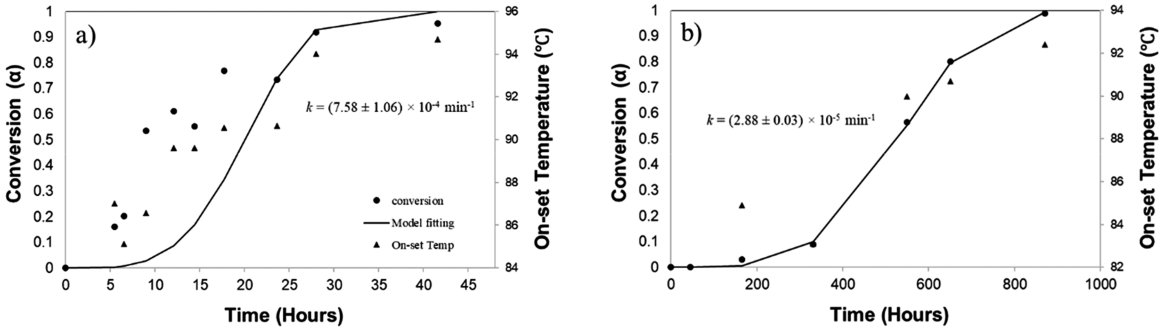

Figure 5. Plots of fractional conversion versus time during polymorphic transition of form 2 → form 1 at room temperature (20 °C): (a) polycrystalline; (b) powder samples. Each data point for fractional conversion (left *y*-axis) and onset temperature (right *y*-axis) at the measured time are marked by triangle symbols (▲) and circle symbols (●) respectively. The temperature-dependent rate constants (k) of two forms were determined by linear Avrami-Erofeev (n = 4) model fitting.

formed.[35] According to Mnyukh's one-by-one theory, the activation energy of phase propagation (E_s) is 0.7 times smaller than the enthalpy of sublimation when the effective gap between the phase is assumed to be 0.5 molecular layer.[35] The global activation energy of SSPT is comprised of activation energies of elementary steps (nucleation and phase propagation). Our large value observed for the global activation energy might be reasonable if we consider that the activation energy for the nucleation step is typically expected to be much higher than the one for a phase propagation step.[24] It is also noted that large activation energy in the phase transition was previously illustrated with another point of view. In recent work conducted by Farasat et al, the large activation energy of melting of glucose was interpreted as the result of a cooperative mechanism, and the number of molecules involved in a cooperative phase transition was determined based on the relation between activation energy and the heat of melting.[62]

In addition, the result that the activation energy of form 1 → form 2 transition obtained with polycrystalline samples was larger than that obtained with powders showed that a lower activation energy is not always a prerequisite for higher transition rates. We might conclude that the lower global activation energy barrier observed in powder samples might be due to the inclusion of more lattice defects during preparation of powders by grinding polycrystalline samples. Meanwhile, the lower transition rates observed in powder samples are likely associated with the generation of a large number of small crystallites during preparation of the samples by grinding, which requires more nucleation events.

The dependence of crystal forms (powders and polycrystalline) on the transition rate and DSC measurements of the reverse transition under isothermal conditions (20 °C) was also studied by the following procedures: (i) the enthalpies for the forward transition (form 1 → form 2) of multiple samples were first obtained by nonisothermal DSC runs (β = 1 K min $^{-1}$); (ii) each sample (which was completely converted to form 2 by previous DSC runs) was kept at room temperature (20 °C) with various incubation times; (iii) the enthalpy of form 1 → form 2 transition of samples was subsequently remeasured by non-isothermal DSC runs (β = 1 K min $^{-1}$); (iv) fractional conversions of each sample for the reverse transition (form 2 → form 1) with time at the 20 °C were obtained by comparing the enthalpies calculated from (i) and (iii).

Figure 5 shows the fractional conversion (α)-versus-time curves of the reverse transition at 20 °C using polycrystalline (Figure 5a) and powders (Figure 5b). The onset temperature of each sample measured in subsequent DSC runs (iii) were also described in the right *y*-axis, along with extent of conversion (α). The conversion rates of powders were much slower compared to polycrystalline as previously shown in the forward transition. The temperature-dependent rate constant (k) of the two forms were obtained by linear Avrami-Erofeev (n = 4) model fitting (polycrystalline: $(7.58 \pm 1.06) \times 10^{-4}$ min^{-1}; powders: $(2.88 \pm 0.03) \times 10^{-5}$ min^{-1}). The rate constant of powders was relatively well matched with the

DOI: 10.1021/acs.cgd.8b01488
Cryst. Growth Des. 2019, 19, 932−941

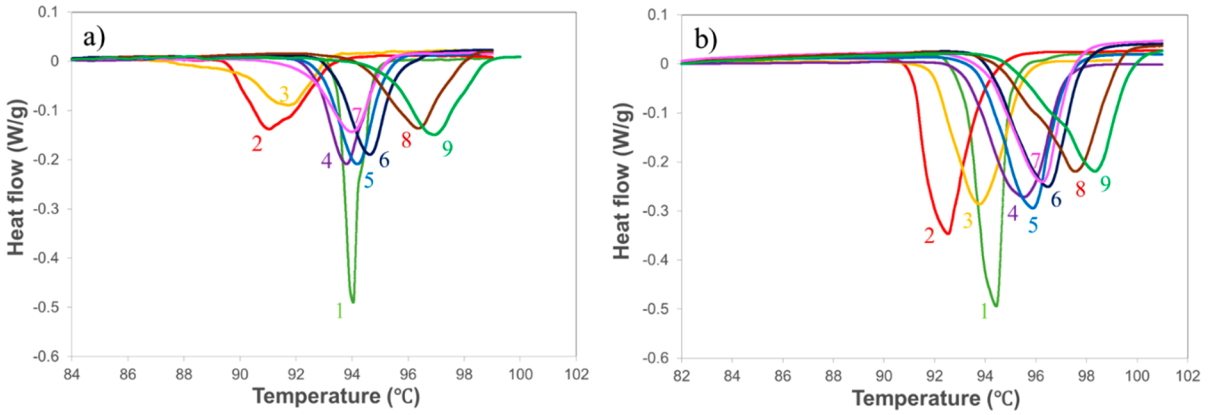

Figure 6. Change of non-isothermal DSC patterns for form 1 → form 2 transition using poly crystalline according to repeated transition cycles: (a) at β = 0.5 K min^{-1} (b) at β = 1 K min^{-1}.

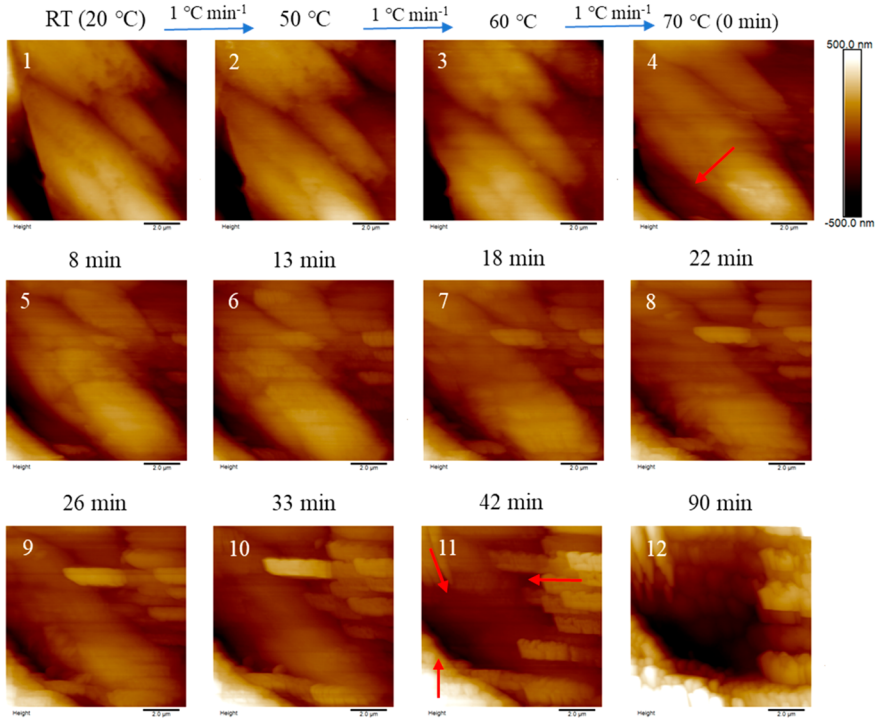

Figure 7. Evolution of AFM height images for the surface of form 1 polycrystalline during heating in the temperature range of 20−70 °C. All images are 10 μm × 10 μm.

values calculated by powder X-ray analysis (k = (6.41 ± 0.11) × 10^{-5} min^{-1}). It is interesting to note that the onset temperature measured in the second cycle of DSC runs (form 1 → form 2) tended to change in accordance with the extent of conversion. This could also illustrate the SSPT mechanism of NA/PA cocrystal being dominated by a nucleation and growth mechanism. When form 2 is not completely converted to form 1 before the resumption of form 1 → form 2 transition, a small degree of superheating (the lower onset temperature) might be sufficient for the phase transition since it is mainly operated by phase propagation. In contrast, a large degree of superheating (higher onset temperature), which is enough to overcome the nucleation energy barrier, might be required for the forward transition in the absence of form 2 phase.

The effects of crystal forms and defect inclusions on the kinetics of the SSPT process were also investigated in another DSC experiment. Figure 6 shows the change of non-isothermal DSC patterns for the forward transition using polycrystalline samples as the number of transition cycles increases. Before repeating each cycle of DSC run, samples were held at room temperature for 7 days such that form 2 would be completely converted to form 1. The enthalpy of transition for each run was 9.6 ± 0.7 kJ mol^{-1} at β = 0.5 K min^{-1} and 9.2 ± 0.4 kJ mol^{-1} at β = 1 K min^{-1}. In the successive heating of form 1 → form 2 transitions, sharp DSC pattern, initially observed, tended to become broader, as observed in DSC patterns of powders shown in Figure 3. SEM images show that the large number of small crystals or grains were formed on the polycrystalline surface during transitions (see Supporting Information, Figure S6). The observed transition points also changed upon the successive repeating cycles. In the second heating run, the transition point was shifted to the left, toward a lower temperature, which showed that transition becomes more favorable. This is probably the result of the release of

DOI: 10.1021/acs.cgd.8b01488
Cryst. Growth Des. 2019, 19, 932−941

strain within the crystallites during heating associated with nucleation of different crystal structures of the new phase (form 2). In the subsequent repeating cycles, however, the transition curve shifted to the right, toward higher temperatures, as the samples became degraded upon the successive heating/cooling cycles.

3.3. In Situ AFM. AFM analysis was conducted to monitor the surface morphology change upon the polymorphic transition. In an attempt to visualize this phenomena, nucleation, and growth of the new phase, hot stage microscopy is often used in SSPT studies.[31,42,44,70] Compared to hot stage microscopy, in situ AFM is beneficial in the ease of sample preparation and detection of the morphological change with high spatial resolution at very early times. Figure 7 shows the evolution of the surface change of form 1 polycrystalline with time and temperature. The temperature ramping rate was set to 1 K min^{-1} to reduce the thermal drift and to identify the temperature where the morphology started to change. No change of crystal surface was observed up to 60 °C (images 1−3, Figure 7). However, the surface morphology started to change when the temperature increased from 60 to 70 °C (image 4, Figure 7). The appearance of new structures was observed (images 5−12, Figure 7) when the sample was constantly heated at 70 °C. The direction of formation and the growth of new structures were in random orientations (image 11, Figure 7). Above 70 °C, it was no longer possible to image the surface evolution due to the fast rate of growth and damage to the AFM tip. These experiments were repeated with two other polycrystalline, and the initiation of surface change was also observed close to 70 °C.

As observed in Figure 7, the formation and growth of new structures were observed during heating of form 1 in the AFM. Interestingly, the onset temperature (∼70 °C) where the surface modification was initiated was lower than that from the DSC analysis. In a recent study on the solid-state polymorphic transition of Irganox 1076, AFM was used to unveil a hidden solid phase transition which was not detected with classical tools, FT-IR and DSC.[53] In this study, the formation and disappearance of the structures were observed on the crystal surface during the transition. Saunier et al. suggested that the AFM tip might cause a high local pressure on the crystal surface inducing the phase transition locally in the AFM at mild temperatures.[53] The effect of the AFM tip on the kinetic process of other solid-state reactions was also observed in the crystallization of amorphous droplets of organic molecules where crystallization was induced by tip/surface interaction during AFM scanning.[71,72] In this sense, it might be possible that the AFM tip can act as a secondary nucleation medium and accelerate the kinetic process of SSPT process in the very local areas. Or, impurities, such as individual molecules forming the cocrystal, could be reasons that we see surface morphology changes in the AFM at such low temperatures. However, there is no evidence that the formation of new structures is associated with a polymorphic transition because the two different phases of structures are not distinguishable in AFM. In addition, the onset temperature of the surface morphology change observed in the AFM (70 °C) is much lower than the transition point obtained by slurry tests conducted by Aitipamula et al. (85−90 °C).[44] Further investigation and the development of AFM to distinguish polymorphs are needed for AFM to be utilized as an alternative tool to detect polymorphic transitions.

4. CONCLUSION

In this work, the kinetics of enantiotropic solid-state polymorphic transitions between form 1 and form 2 of 1:1 nicotinamide (NA)/pimelic acid (PA) cocrystals were investigated. Bulk kinetic studies conducted with PXRD and DSC indicated that solid-state polymorphic transition of NA/PA cocrystals occurs by a nucleation and growth mechanism where superheating or supercooling is essential for the initiation of the transition process. In the kinetic transition PXRD experiment, both directions of transition behavior of form 1 ↔ form 2 were well described by the Avrami-Erofeev model. In the DSC analysis with two crystal forms (polycrystalline and powders), large activation energies were observed with a wide range (337.1−514.2 kJ mol^{-1}). Also, the change of transition points for form 1 → form 2 with the number of transition cycling was observed in polycrystalline samples of form 1, which might be attributed to the defect inclusions and the degradation of polycrystalline samples during the transition process. We also observed the surface morphology changes of form 1 during the transitions through the in situ AFM while we increased the temperature. Interestingly, the temperature where the formation of new structures on the surface initiates was observed with AFM (possibly related to polymorphic transition) was much lower than the observed transition temperature, as measured by bulk kinetic methods. We failed to find evidence that the surface morphology change is related to transition of two polymorphs. However, this finding should not exclude a possible AFM tip effect on the kinetics of polymorphic transitions.

■ ASSOCIATED CONTENT

Supporting Information

The Supporting Information is available free of charge on the ACS Publications website at DOI: 10.1021/acs.cgd.8b01488.

PXRD patterns, SEM images, and thermal analysis data (PDF)

■ AUTHOR INFORMATION

Corresponding Author

*Address: Department of Chemical Engineering, Texas Tech University, Lubbock, Texas 79409, USA. E-mail: brandon.weeks@ttu.edu.

ORCID

Yong Joon Lee: 0000-0002-5308-9120

Notes

The authors declare no competing financial interest.

■ ACKNOWLEDGMENTS

We thank Dr. Daniel Unruh (Senior Research Associate, Department of Chemistry, Texas Tech University) for assistance in the collection of PXRD data.

■ REFERENCES

(1) Bernstein, J. *Polymorphism in Molecular Crystals*; Oxford University Press: New York, 2002.

(2) Schultheiss, N.; Newman, A. Pharmaceutical Cocrystals and Their Physicochemical Properties. *Cryst. Growth Des.* **2009**, *9*, 2950−2967.

(3) Qiao, N.; Li, M.; Schlindwein, W.; Malek, N.; Davies, A.; Trappitt, G. Pharmaceutical Cocrystals: An Overview. *Int. J. Pharm.* **2011**, *419*, 1−11.

(4) Desiraju, G. R. Crystal Engineering: From Molecule to Crystal. *J. Am. Chem. Soc.* **2013**, *135*, 9952−9967.
(5) Najar, A. A.; Azim, Y. Pharmaceutical Co-Crystals: A New Paradigm of Crystal Engineering. *J. Indian Inst. Sci.* **2014**, *94*, 45−67.
(6) Miroshnyk, I.; Mirza, S.; Sandler, N. Pharmaceutical Co-Crystals-an Opportunity for Drug Product Enhancement. *Expert Opin. Drug Delivery* **2009**, *6*, 333−341.
(7) Brittain, H. G. Cocrystal Systems of Pharmaceutical Interest: 2011. *Cryst. Growth Des.* **2012**, *12*, 5823−5832.
(8) Cherukuvada, S.; Kaur, R.; Guru Row, T. N. Co-Crystallization and Small Molecule Crystal Form Diversity: From Pharmaceutical to Materials Applications. *CrystEngComm* **2016**, *18*, 8528−8555.
(9) Izutsu, K.; Koide, T.; Takata, N.; Ikeda, Y.; Ono, M.; Inoue, M.; Fukami, T.; Yonemochi, E. Characterization and Quality Control of Pharmaceutical Cocrystals. *Chem. Pharm. Bull. (Tokyo)* **2016**, *64*, 1−12.
(10) Healy, A. M.; Worku, Z. A.; Kumar, D.; Madi, A. M. Pharmaceutical Solvates, Hydrates and Amorphous Forms: A Special Emphasis on Cocrystals. *Adv. Drug Delivery Rev.* **2017**, *117*, 25−46.
(11) Karpinski, P. H. Polymorphism of Active Pharmaceutical Ingredients. *Chem. Eng. Technol.* **2006**, *29*, 233−237.
(12) Raza, K.; Kumar, P.; Ratan, S.; Malik, R.; Arora, S. Polymorphism : The Phenomenon Affecting the Performance of Drugs. *SOJ. Pharm. Pharm. Sci.* **2014**, *1*, 1−10.
(13) Lee, E. H. A Practical Guide to Pharmaceutical Polymorph Screening & Selection. *Asian J. Pharm. Sci.* **2014**, *9*, 163−175.
(14) Llinàs, A.; Goodman, J. M. Polymorph Control: Past, Present and Future. *Drug Discovery Today* **2008**, *13*, 198−210.
(15) Chemburkar, S. R.; Bauer, J.; Deming, K.; Spiwek, H.; Patel, K.; Morris, J.; Henry, R.; Spanton, S.; Dziki, W.; Porter, W.; et al. Dealing with the Impact of Ritonavir Polymorphs on the Late Stages of Bulk Drug Process Development. *Org. Process Res. Dev.* **2000**, *4*, 413−417.
(16) Jiang, S.; Jansens, P. J.; Ter Horst, J. H. Control over Polymorph Formation of O-Aminobenzoic Acid. *Cryst. Growth Des.* **2010**, *10*, 2541−2547.
(17) Su, W.; Hao, H.; Barrett, M.; Glennon, B. The Impact of Operating Parameters on the Polymorphic Transformation of D-Mannitol Characerized in Situ with Raman Spectroscopy, FBRM, and PVM. *Org. Process Res. Dev.* **2010**, *14*, 1432−1437.
(18) O'Mahony, M. A.; Maher, A.; Croker, D. M.; Rasmuson, Å. C.; Hodnett, B. K. Examining Solution and Solid State Composition for the Solution-Mediated Polymorphic Transformation of Carbamazepine and Piracetam. *Cryst. Growth Des.* **2012**, *12*, 1925−1932.
(19) Aucamp, M.; Stieger, N.; Barnard, N.; Liebenberg, W. Solution-Mediated Phase Transformation of Different Roxithromycin Solid-State Forms: Implications on Dissolution and Solubility. *Int. J. Pharm.* **2013**, *449*, 18−27.
(20) Du, W.; Yin, Q.; Hao, H.; Bao, Y.; Zhang, X.; Huang, J.; Li, X.; Xie, C.; Gong, J. Solution-Mediated Polymorphic Transformation of Prasugrel Hydrochloride from Form II to Form I. *Ind. Eng. Chem. Res.* **2014**, *53*, 5652−5659.
(21) Mnyukh, Y. V.; Panfilova, N. A.; Petropavlov, N. N.; Uchvatova, N. S. Polymorphic Transitions in Molecular Crystals-III. Transitions Exhibiting Unusual Behavior. *J. Phys. Chem. Solids* **1975**, *36*, 127−144.
(22) Mnyukh, Y. V. Polymorphic Transitions in Crystals: Kinetics. *Mol. Cryst. Liq. Cryst.* **1979**, *52*, 201−217.
(23) Smilowitz, L.; Henson, B. F.; Asay, B. W.; Dickson, P. M. The β-δ Phase Transition in the Energetic Nitramine-Octahydro-1,3,5,7-Tetranitro-1,3,5,7-Tetrazocine: Kinetics. *J. Chem. Phys.* **2002**, *117*, 3789−3798.
(24) Burnham, A. K.; Weese, R. K.; Weeks, B. L. Distributed Activation Energy Model of Thermodynamically Inhibited Nucleation and Growth Reactions and Its Application to the β−δ Phase Transition of HMX. *J. Phys. Chem. B* **2004**, *108*, 19432−19441.
(25) Li, J.; Brill, T. B. Kinetics of Solid Polymorphic Phase Transitions of CL-20. *Propellants, Explos., Pyrotech.* **2007**, *32*, 326−330.
(26) Kishi, Y.; Matsuoka, M. Phenomena and Kinetics of Solid-State Polymorphic Transition of Caffeine. *Cryst. Growth Des.* **2010**, *10*, 2916−2920.
(27) Stilinovic, V.; Kaitner, B. Structural and Thermodynamic Insight into Solid State Phase Transition Mechanism of a 1, 3, 3 ′ -Triketone. *Cryst. Growth Des.* **2013**, *13*, 1703−1711.
(28) Zakharov, V. V.; Chukanov, N. V.; Chervonnyi, A. D.; Vozchikova, S. A.; Korsounskii, B. L. Kinetics of Reversible Polymorphic Transition in Energetic Materials. Phase Transitions $\alpha \rightarrow \beta$ and $\beta \rightarrow \alpha$ in 1,1-Diamino-2,2-Dinitroethylene. *Russ. J. Phys. Chem. B* **2014**, *8*, 822−828.
(29) Farasat, R.; Yancey, B.; Vyazovkin, S. High Temperature Solid-Solid Transition in Ammonium Chloride Confined to Nanopores. *J. Phys. Chem. C* **2013**, *117*, 13713−13721.
(30) Farasat, R.; Vyazovkin, S. Nanoconfined Solid-Solid Transitions: Attempt to Separate the Size and Surface Effects. *J. Phys. Chem. C* **2015**, *119*, 9627−9636.
(31) Joseph, A.; Bernardes, C. E. S.; Druzhinina, A. I.; Varushchenko, R. M.; Nguyen, T. Y.; Emmerling, F.; Yuan, L.; Dupray, V.; Coquerel, G.; Da Piedade, M. E. M. Polymorphic Phase Transition in 4′-Hydroxyacetophenone: Equilibrium Temperature, Kinetic Barrier, and the Relative Stability of $Z' = 1$ and $Z' = 2$ Forms. *Cryst. Growth Des.* **2017**, *17*, 1918−1932.
(32) Herbstein, F. H. On the Mechanism of Some First-Order Enantiotropic Solid-State Phase Transitions: From Simon through Ubbelohde to Mnyukh. *Acta Crystallogr., Sect. B: Struct. Sci.* **2006**, *62*, 341−383.
(33) Zahn, D.; Anwar, J. Collective Displacements in a Molecular Crystal Polymorphic Transformation. *RSC Adv.* **2013**, *3*, 12810−12815.
(34) Van Den Ende, J. A.; Smets, M. M. H.; De Jong, D. T.; Brugman, S. J. T.; Ensing, B.; Tinnemans, P. T.; Meekes, H.; Cuppen, H. M. Do Solid-to-Solid Polymorphic Transitions in DL-Norleucine Proceed through Nucleation? *Faraday Discuss.* **2015**, *179*, 421−436.
(35) Mnyukh, Y. V. *Fundamentals of Solid-State Phase Transitions, Ferromagnetism and Ferroelectricity*; 1st Books Library, Bloomington, 2001.
(36) Ubbelohde, A. R. Geometrical Representation of Thermal Transitions of Higher Order. *Nature* **1952**, *169*, 832.
(37) Ubbelohde, A. R. Crystallography and the Phase Rule. *Br. J. Appl. Phys.* **1956**, *7*, 313−321.
(38) Aitipamula, S.; Chow, P. S.; Tan, R. B. H. Polymorphism in Cocrystals: A Review and Assessment of Its Significance. *CrystEngComm* **2014**, *16*, 3451−3465.
(39) Trask, A. V.; Van De Streek, J.; Motherwell, W. D. S.; Jones, W. Achieving Polymorphic and Stoichiometric Diversity in Cocrystal Formation: Importance of Solid-State Grinding, Powder X-Ray Structure Determination, and Seeding. *Cryst. Growth Des.* **2005**, *5*, 2233−2241.
(40) Childs, S. L.; Hardcastle, K. I. Cocrystals of Chlorzoxazone with Carboxylic Acids. *CrystEngComm* **2007**, *9*, 364.
(41) Aitipamula, S.; Chow, P. S.; Tan, R. B. H. Polymorphs and Solvates of a Cocrystal Involving an Analgesic Drug, Ethenzamide, and 3,5-Dinitrobenzoic Acid. *Cryst. Growth Des.* **2010**, *10*, 2229−2238.
(42) Vangala, V. R.; Chow, P. S.; Schreyer, M.; Lau, G.; Tan, R. B. H. Thermal and in Situ X-Ray Diffraction Analysis of a Dimorphic Co-Crystal, 1:1 Caffeine-Glutaric Acid. *Cryst. Growth Des.* **2016**, *16*, 578−586.
(43) Hasa, D.; Carlino, E.; Jones, W. Polymer-Assisted Grinding, a Versatile Method for Polymorph Control of Cocrystallization. *Cryst. Growth Des.* **2016**, *16*, 1772−1779.
(44) Aitipamula, S.; Wong, A. B.; Chow, P. S.; Tan, R. B. Polymorphism and phase transformations of a cocrystal of nicotinamide and pimelic acid. *CrystEngComm* **2012**, *14*, 8193−8198.
(45) Khawam, A.; Flanagan, D. R. Solid-State Kinetic Models: Basics and Mathematical Fundamentals. *J. Phys. Chem. B* **2006**, *110*, 17315−17328.

DOI: 10.1021/acs.cgd.8b01488
Cryst. Growth Des. 2019, 19, 932−941

(46) Yaji, T.; Yoshida, K.; Isoda, S.; Kobayashi, T.; Sato, N.; Shirotani, I. Atomic Force Microscopic Observation of Phase Transformation Process of bis(1,2-benzoquinonedioximato)platinum-(II). *Thin Solid Films* **2001**, *393*, 319−324.
(47) Weeks, B. L.; Ruddle, C. M.; Zaug, J. M.; Cook, D. J. Monitoring High-Temperature Solid − Solid Phase Transitions of HMX with Atomic Force Microscopy. *Ultramicroscopy* **2002**, *93*, 19−23.
(48) Ito, A.; Yamanobe-Hada, M.; Shindo, H. In Situ AFM Observation of Polymorphic Transformation at Crystal Surface of Glycine. *J. Cryst. Growth* **2005**, *275*, e1691−e1695.
(49) Jones, M. D.; Beezer, A. E.; Buckton, G. Determination of Outer Layer and Bulk Dehydration Kinetics of Trehalose Dihydrate Using Atomic Force Microscopy, Gravimetric Vapour Sorption and Near Infrared Spectroscopy. *J. Pharm. Sci.* **2008**, *97* (10), 4404−4415.
(50) Chen, D.; Haugstad, G.; Li, Z. J.; Suryanarayanan, R. Water Sorption Induced Transformations in Crystalline Solid Surfaces: Characterization by Atomic Force Microscopy. *J. Pharm. Sci.* **2010**, *99*, 4032−4041.
(51) Chow, E. H. H.; Bučar, D.-K.; Jones, W. New Opportunities in Crystal Engineering − the Role of Atomic Force Microscopy in Studies of Molecular Crystals. *Chem. Commun.* **2012**, *48*, 9210.
(52) Thakuria, R.; Eddleston, M. D.; Chow, E. H. H.; Lloyd, G. O.; Aldous, B. J.; Krzyzaniak, J. F.; Bond, A. D.; Jones, W. Use of In Situ Atomic Force Microscopy to Follow Phase Changes at Crystal Surfaces in Real Time. *Angew. Chem.* **2013**, *125*, 10735−10738.
(53) Saunier, J.; Herry, J.-M.; Yagoubi, N.; Marlière, C. Exploring Complex Transitions between Polymorphs on a Small Scale by Coupling AFM, FTIR and DSC: The Case of Irganox 1076® Antioxidant. *RSC Adv.* **2017**, *7*, 3804−3818.
(54) Vyazovkin, S.; Burnham, A. K.; Criado, J. M.; Pérez-Maqueda, L. A.; Popescu, C.; Sbirrazzuoli, N. ICTAC Kinetics Committee Recommendations for Performing Kinetic Computations on Thermal Analysis Data. *Thermochim. Acta* **2011**, *520*, 1−19.
(55) Vyazovkin, S.; Chrissafis, K.; Di Lorenzo, M. L.; Koga, N.; Pijolat, M.; Roduit, B.; Sbirrazzuoli, N.; Suñol, J. J. ICTAC Kinetics Committee Recommendations for Collecting Experimental Thermal Analysis Data for Kinetic Computations. *Thermochim. Acta* **2014**, *590*, 1−23.
(56) Volmer, M.; Weber, Z. Keimbildung in übersättigten Gebilden. *Z. Phys. Chem.* **1926**, *119*, 277−301.
(57) Turnbull, D.; Fisher, J. C. Rate of Nucleation in Condensed Systems. *J. Chem. Phys.* **1949**, *17*, 71−73.
(58) Papon, P.; Leblond, J.; Meijer, P. H. E. *The Physics of Phase Transitions*; Springer: Berlin, 2002.
(59) Christian, J. W. *The Theory of Transformations in Metals and Alloys*; Pergamon, Amsterdam, 2002.
(60) Mullin, J. W. *Crystallization*; Elsevier Butterworth-Heinemann, Oxford, 4th edn, 2004.
(61) Anwar, J.; Zahn, D. Polymorphic Phase Transitions: Macroscopic Theory and Molecular Simulation. *Adv. Drug Delivery Rev.* **2017**, *117*, 47−70.
(62) Liavitskaya, T.; Birx, L.; Vyazovkin, S. Melting Kinetics of Superheated Crystals of Glucose and Fructose. *Phys. Chem. Chem. Phys.* **2017**, *19*, 26056−26064.
(63) De Bruijn, T. J. W.; De Jong, W. A.; Van Den Berg, P. J. Kinetic Parameters in Avrami-Erofeev Type Reactions from Isothermal and Non-isothermal experiments. *Thermochim. Acta* **1981**, *45*, 315−325.
(64) Politzer, P.; Concha, M. C.; Grice, M. E.; Murray, J. S.; Lane, P. Computational Investigation of the Structures and Relative Stabilities of Amino/Nitro Derivatives of Ethylene. *J. Mol. Struct.: THEOCHEM* **1998**, *452*, 75−83.
(65) Burnham, A. K.; Weese, R. K.; Wang, R.; Kwok, Q. S. M.; Jones, D. E. G. Solid-Solid Phase Transition Kinetics of Fox-7; In *Proceedings 33rd Annual Conference of the North American Thermal Analysis Society (NATAS)*; Universal City: USA, 2005; pp 287−294.
(66) Rong, H. R.; Gu, H. Polymorphs of 2,4,5,6-Tetrachloro-1,3-Benzenedicarbonitile and their Transformations. *Thermochim. Acta* **2005**, *428*, 19−23.
(67) Surov, A. O.; Terekhova, I. V.; Bauer-Brandl, A.; Perlovich, G. L. Thermodynamic and Structural Aspects of Some Fenamate Molecular Crystals. *Cryst. Growth Des.* **2009**, *9*, 3265−3272.
(68) Gilpin, R. K.; Zhou, W. J. Infrared Studies of the Polymorphic States of the Fenamates. *J. Pharm. Biomed. Anal.* **2005**, *37*, 509−515.
(69) Gilpin, R. K.; Zhou, W. Vib. Infrared Studies of the Thermal Conversion of Mefenamic Acid between Polymorphic States. *Vib. Spectrosc.* **2005**, *37*, 53−59.
(70) Smets, M. M. H.; Brugman, S. J. T.; Van Eck, E. R. H.; Van Den Ende, J. A.; Meekes, H.; Cuppen, H. M. Understanding the Solid-State Phase Transitions of Dl-Norleucine: An in Situ DSC, Microscopy, and Solid-State NMR Study. *Cryst. Growth Des.* **2015**, *15*, 5157−5167.
(71) Zhang, G.; Weeks, B. L. Inducing Dendrite Formation Using an Atomic Force Microscope Tip. *Scanning* **2008**, *30*, 228−231.
(72) Zhang, X.; Weeks, B. L. Tip Induced Crystallization Lithography Tip Induced Crystallization Lithography. *J. Am. Chem. Soc.* **2014**, *136*, 1253−1255.

DOI: 10.1021/acs.cgd.8b01488
Cryst. Growth Des. 2019, 19, 932−941